PROCEEDINGS OF SPIE

SPIEDigitalLibrary.org/conference-proceedings-of-spie

# In vivo quantitative evaluation of gold nanocages' kinetics in sentinel lymph nodes by photoacoustic tomography

Xin Cai, Weiyang Li, Chulhong Kim, Yuchen Yuan, Younan Xia, et al.

Xin Cai, Weiyang Li, Chulhong Kim, Yuchen Yuan, Younan Xia, Lihong V. Wang, "In vivo quantitative evaluation of gold nanocages' kinetics in sentinel lymph nodes by photoacoustic tomography," Proc. SPIE 8223, Photons Plus Ultrasound: Imaging and Sensing 2012, 82233P (23 February 2012); doi: 10.1117/12.909281

SPIE.

Event: SPIE BiOS, 2012, San Francisco, California, United States

Downloaded From: https://www.spiedigitallibrary.org/conference-proceedings-of-spie on 9/18/2018 Terms of Use: https://www.spiedigitallibrary.org/terms-of-use

# *In Vivo* Quantitative Evaluation of Gold Nanocages' Kinetics in Sentinel Lymph Nodes by Photoacoustic Tomography

Xin Cai, Weiyang Li, Chulhong Kim, Yuchen Yuan, Younan Xia, and Lihong V. Wang*

Optical Imaging Laboratory, Department of Biomedical Engineering, Washington University in St. Louis, St. Louis, Missouri 63130

## ABSTRACT

As a new class of sentinel lymph node (SLN) tracers for photoacoustic (PA) imaging, Au nanocages offer the advantages of noninvasiveness, strong optical absorption in the near-infrared region (for deep penetration), and accumulation in higher concentrations than the initial injected solution. By monitoring the amplitude changes of PA signals in an animal model, we quantified the accumulations of nanocages in SLNs over time. Based on this method, we quantitatively evaluated the kinetics of gold nanocages in SLN in terms of concentration, size, and surface modification. We could detect the SLN at an Au nanocage injection concentration of 50 pM and a dose of 100 μL *in vivo*. This concentration is about 40 times less than the previously reported value. We also investigated the influence of nanocages' size (50 nm and 30 nm in edge length), and the effects of surface modification (with positive, or neutral, or negative surface charges). The results are helpful to develop this AuNC-based PA imaging system for noninvasive lymph node mapping, providing valuable information about metastatic cancer staging.

**Keywords:** Gold nanocages; sentinel lymph node; photoacoustic tomography.

## 1. INTRODUCTION

The metastatic spread of cancer cells occurs by invading the adjacent tissue and disseminating in the blood stream *via* the lymphatic system.[1] The closest lymph node that receives the drainage from a cancer-containing area is called the sentinel lymph node (SLN). The SLN represents the most possible first location of metastatic spread. To reduce the side effects of axillary lymph node dissection,[2] sentinel lymph node biopsy (SLNB) is widely performed and has become the standard for axillary staging in breast cancer patients.[3] However, SLNB requires ionizing imaging and is invasive.

Recently, ultrasound-guided fine needle aspiration biopsy (FNAB) has been clinically evaluated as a minimally invasive procedure.[4] This technique requires accurate identification of the SLN, which initiates studies to develop accurate, nonionizing, and noninvasive methods for SLN mapping. Photoacoustic (PA) imaging modality is a nonionizing, noninvasive, and high-resolution imaging technique that provides strong optical absorption contrast.[5,6] Since the spatial resolution of this technique typically depends on ultrasound parameters, the imaging depth can be extended to the optical quasidiffusive or diffusive regime while keeping high resolution. It can achieve up to ~50 mm imaging depth in biological tissues.[7]

* Corresponding author: lhwang@biomed.wustl.edu

Photons Plus Ultrasound: Imaging and Sensing 2012, edited by Alexander A. Oraevsky, Lihong V. Wang,
Proc. of SPIE Vol. 8223, 82233P · © 2012 SPIE · CCC code: 1605-7422/12/$18 · doi: 10.1117/12.909281



Downloaded From: https://www.spiedigitallibrary.org/conference-proceedings-of-spie on 9/18/2018
Terms of Use: https://www.spiedigitallibrary.org/terms-of-use

Gold nanocages (AuNCs), which are hollow porous nanoparticles, have proper size range (30–100 nm) to stay within the SLN with secure fast migration and sufficient duration of trapping for imaging.[8] AuNCs also can be utilized effectively for delivering and targeting because of their easily modifiable surfaces.[9,10] Other advantages of AuNCs include biocompatibility, a lack of heavy metal toxicity, a tunable localized surface plasmon resonance (LSPR) peak, encapsulated site-specific drug delivery,[11] and strong optical absorption in the near inferred spectral region. Moreover, gold has been approved and used for various phase-I clinical trials (e.g., http://www.cytimmune.com and http://www.nanospectra.com). These features suggest AuNC a promising candidate as contrast agent in the PA SLN mapping. Our previous work has successfully demonstrated a proof-of-concept use of AuNCs for SLN imaging by PA tomography.[12] However, many parameters still need to be examined and optimized before this system can be further considered for potential clinical use. In the present paper, we quantitatively evaluated *in vivo* kinetics of AuNCs in lymphatic systems by PA imaging on a rat model. The influences of the injection concentration, the size, and the surface charge were systematically examined. These evaluations are helpful to optimize the experimental parameters of AuNCs for lymph node metastases by *in vivo* noninvasive PA mapping.

## 2. MATERIALS AND METHODS

### 2.1 Synthesis and Surface Modification of AuNCs

The method The Au nanocages were synthesized using the galvanic replacement reaction between Ag nanocubes and chloroauric acid in water according to our published protocol.[13] To obtain different surface charges, the nanocages were derivatized with SH-$PEG_{5000}$-X (X=OMe, $NH_2$, and COOH; all from Laysan Bio; Mw ≈ 5,000). In a typical process, 0.1 mL of HS-$PEG_{5000}$-X aqueous solution (0.1 mM) and 0.1 mL of AuNCs aqueous suspension (1 nM in terms of particles) were added to 2.8 mL deionized water. The mixture was kept stirring at 4 $^{o}$C overnight. After that, the mixture was centrifuged at 14,000 rpm for 15 min and the supernatant was decanted to remove the excess PEG. The PEGylated-AuNCs were then washed with water twice and re-suspended in water at a concentration of 200 pM (in terms of particles) for *in vivo* studies.

### 2.2 Photoacoustic Tomography System

A reflection-mode PA imaging system (Scheme 1 in ref. 14) was used for all PA experiments. [14] *Light source*: tunable Ti:sapphire laser (760nm, LT-2211A, LOTIS TII) pumped by a Q-switched Nd:YAG (LS- 2137/2, LOTIS TII); pulse width <15 ns, pulse repetition rate 10 Hz. The incident laser fluence on the sample surface was controlled to conform to the American National Standards Institute standards. *Transducer*: 5 MHz central frequency, spherically focused, 2.54 cm focul length; 1.91 cm diameter active area element, 72% bandwidth (V308, Panametrics-NDT); low-noise amplifier (5072PR, Panametrics- NDT). Data were acquired with a digital oscilloscope (TDS 5054, Tektronix).

### 2.3 Animal Handling

All animal experiments were in compliance with the Washington University Institutional Animal Care and Use Committee. Sprague–Dawley rats weighting 200–300 g (Harlan, Indianapolis, IN) were anesthetized with ketamine and xylazine cocktail (87 mg/kg and 13 mg/kg, respectively, i.p.) at a dose of 0.15 mL per 100 g body weight. The hair in the left axillary region was removed by gentle clipping and depilatory cream before imaging. PA imaging was achieved before and after a 0.1 mL intradermal injection of AuNC solution in the left forepaw pad. Full anesthesia of the animal was maintained throughout the experiment by using vaporized isoflurane (1 L/min of oxygen and 0.75% isoflurane), and vitals were monitored by a pulse oximeter (NOMIN Medical INC., 2000SA). The body temperatures of the rats were maintained by a water heating pad. After the imaging acquisition, the rats were euthanized by overdosed pentobarbital.



Downloaded From: https://www.spiedigitallibrary.org/conference-proceedings-of-spie on 9/18/2018
Terms of Use: https://www.spiedigitallibrary.org/terms-of-use

## 3. RESULTS AND DISCUSSION

The main objective of this study is to quantitatively investigate the PA contrast enhancement in SLNs provided by AuNCs with different concentrations, sizes, and surface characteristics. To evaluate the *in vivo* sensitivity of our PA system and AuNCs for lymph node imaging, we intradermally injected an aqueous suspension of AuNCs at a specific, decreasing concentration (500, 200, and 50 pM) at a dose of 100 µL on the left forepaw pad of a rat and then the left axillary region of the rat was noninvasively imaged using the PA system. The field of view that possibly contains SLN was chosen based on our previous experience with lymph node imaging.[12] Before the injection of AuNCs, PA images were acquired as control images (Fig. 1A), revealing the vasculature within ~3 mm below the skin surface. After the injection of AuNCs, a series of PA images were obtained up to 120 min post-injection. Fig 1, A–C, show PA images of the axillary region of a rat acquired at 0, 5, and 120 min after injection of the AuNCs with 50 pM × 100 µL. It can be observed that the SLNs started to appear at 5 min after the injection (Fig. 1B). As time elapsed, the PA signals gradually increased and the SLNs could be clearly observed at 120 min post-injection (Fig. 1C). Note that the minimum concentration of 50 pM we used here for PA SLN imaging in a rat model was about 40 times less than the value (2 nM) reported in our previous work,[12] greatly reducing the potential toxicity of AuNCs. The PA signal enhancements in SLNs were summarized as a function of time (Fig. 1D). We found that the PA signal enhancement increased with increasing injection concentration. The enhancement also increased with post-injection time, indicating the gradual accumulation of AuNCs in SLNs. For example, after the injection of 500 pM AuNCs, the enhancement was 406% at t=5 min, and then gradually increased to 647% at t=120 min post-injection.

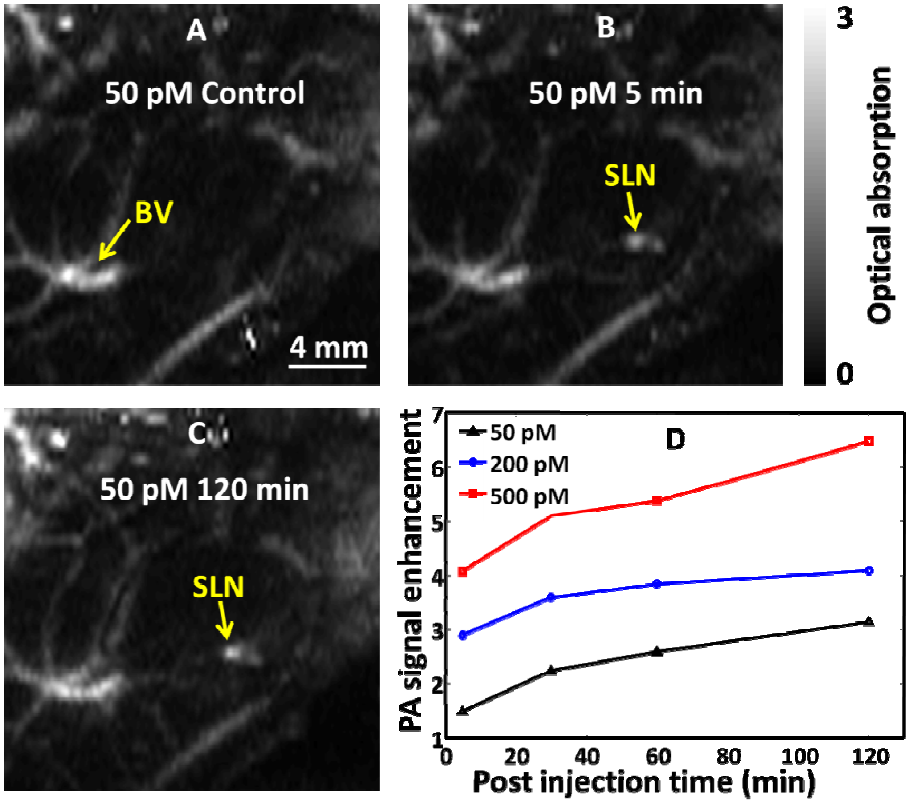


Fig. 1. (A–C) PA images of the axillary region of a rat acquired at 0, 5, and 120 min after injection of the AuNCs with 50 pM × 100 µL. (A) PA image before injection of the AuNCs; (B) PA image at 5 min after the injection of AuNCs. The SLN started to appear; (C) PA image at 120 min after the injection of AuNCs. (D) PA signal enhancement in SLNs as a function of time after the injection of AuNCs at different concentrations: 500, 200, and 50 pM, respectively. BV, blood vessels; SLN, sentinel lymph node.



Downloaded From: https://www.spiedigitallibrary.org/conference-proceedings-of-spie on 9/18/2018
Terms of Use: https://www.spiedigitallibrary.org/terms-of-use

An ideal mapping agent for lymphoscintigraphy should have proper size: on one hand, it should be small enough to rapidly drain to lymphatic vessels and then transport to lymph nodes; on the other hand, it should be large enough to stay within the lymph nodes during the imaging process. Particles smaller than 5 nm could easily leak into blood capillaries or migrate to echelon lymph nodes and thus cause false positives,[15] while particles larger than 100 nm are believed to be trapped in the interstitial compartment for a long period of time, and are thus unable to transport to lymph nodes fast enough for lymphoscintigraphy.[16] Therefore, it is critical to identify an optimal size range for the AuNCs in order to have sufficiently fast migration and sufficient duration of trapping for SLN imaging.

We compared the PA enhancements in SLNs as a function of time using AuNCs with edge lengths of 50 nm and 30 nm, respectively (Fig. 2A). The injection concentrations for both the 30-nm and 50-nm AuNCs were 200 pM (at a dose of 100 μL), as the SLN could hardly be detected with the injection of 30-nm AuNCs at a concentration of 50 pM. Both curves show that SLNs could be detected at 5 min post injection, and the PA signal enhancement kept increasing in the following 120 min. It can be seen that the 50-nm AuNCs showed higher signal enhancement (about 150% to 170%) than the 30-nm sample. This difference can be ascribed to the fact that the 30-nm AuNCs had a smaller optical absorption cross section than the 50-nm AuNCs, generating weaker PA signals. We have also measured the absorption cross sections of these AuNCs using a PA-based method developed in our groups.[17] The absorption cross section of the 50-nm AuNCs was found to be about 2.1 times higher than that of the 30-nm AuNCs. Figure 2C shows typical *in vitro* PA images at the same concentration of 50-nm and 30-nm AuNCs. Figure 2B shows a comparison of the accumulation of 50-nm and 30-nm AuNCs in SLNs as a function of post-injection time calculated from the PA signals. Since the PA signal is directly proportional to the absorption coefficient ($\mu_a$) of the AuNCs, the accumulation of AuNCs can be calculated according to the equation: $N_{nano}=\mu_{a,nano}/\sigma_{a,nano}$, where $N_{nano}$ is the concentration of the AuNCs (number of particles per $m^3$) and $\sigma_{a,nano}$ is the absorption cross section ($m^2$) of the nanocages. It can be seen that the 30-nm AuNCs transported into the SLN faster than the 50-nm AuNCs and showed a larger amount of accumulation in the SLN.

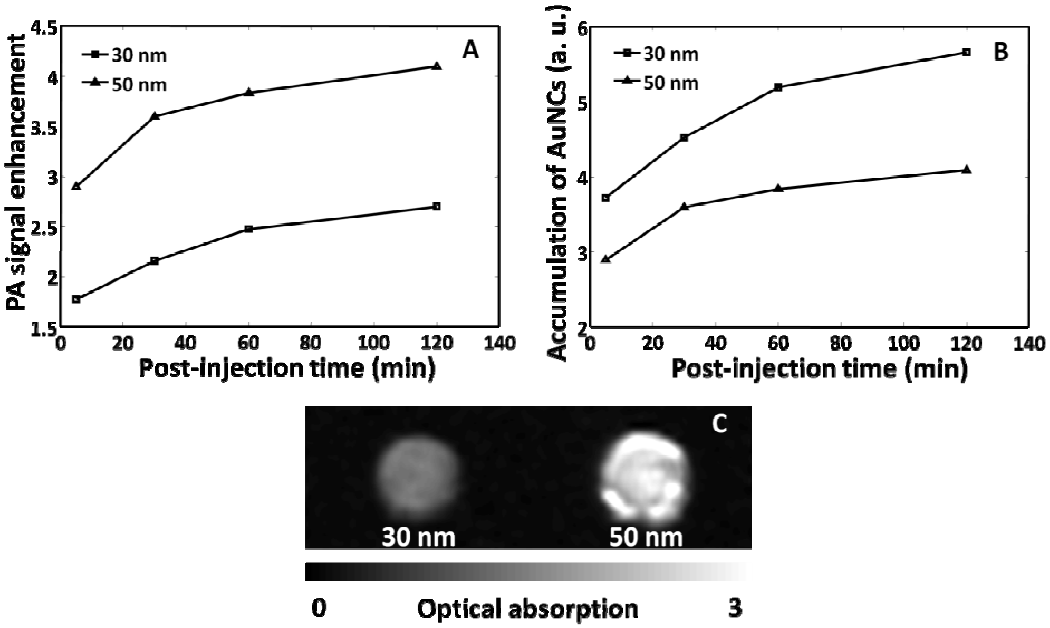


Fig. 2. (A) PA signal enhancement in SLNs after the injection of 50-nm and 30-nm AuNCs with the same concentration and dose (200 pM and 100 μL) as a function of post-injection time, respectively. (B) Accumulation of the 50-nm and 30-nm AuNCs in SLNs as a function of post-injection time calculated based on the PA signals. (C) Typical *in vitro* PA images at the same concentration of 50-nm and 30-nm AuNCs.



Downloaded From: https://www.spiedigitallibrary.org/conference-proceedings-of-spie on 9/18/2018
Terms of Use: https://www.spiedigitallibrary.org/terms-of-use

Early studies on the transport kinetics and lymphatic uptake of particles showed that surface characteristics, such as charge and hydrophobicity, could affect the rate of particle drainage from the injection site to lymph nodes and their distribution within the lymphatic system.[18] Therefore, it is important to study the transport behaviors of AuNCs with different surface charges. We replaced the PVP layer on the AuNCs with SH-PEG5000-X (X=OMe, NH2, or COOH). The zeta-potential of AuNCs covered with SH-$PEG_{5000}$-OMe was about -7.2 mV, and thus the surface charge is considered as neutral. The zeta-potentials of AuNCs covered with SH-$PEG_{5000}$-$NH_2$ and SH-$PEG_{5000}$-COOH were around +12.5 mV and -16.8 mV, giving a relatively positive and negative surface charge, respectively. Following the same procedure, we performed *in vivo* SLN imaging using AuNCs modified with different surface charges. The injection concentration was 200 pM for all 3 groups. Figure 3 shows PA signal enhancement in SLNs as a function of time after the injection of AuNCs with different surface charges. AuNCs with positive charges showed a unique feature. It can be seen that the signal enhancement originating from AuNCs with positive charges is much lower than that from the neutral AuNCs, especially in the first 60 min post injection, indicating a much slower transport rate to lymph nodes. As for the PA enhancement from the AuNCs with negative charges, it was also lower (about 50% to 60%) than the neutral AuNCs, but higher (about 150% to 160%) than the positive AuNCs in the first 60 min post injection, and then leveled off.

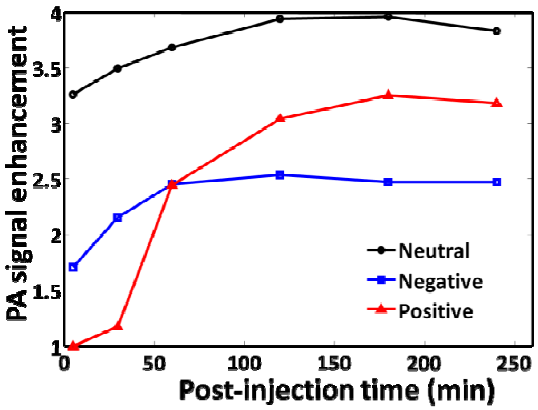


Fig. 3. PA signal enhancement in SLNs as a function of time post injection of AuNCs with different surface charges: negative (blue line), positive (red line), and neutral (black line).

## 4. CONCLUSION

We have quantitatively evaluated the transport of AuNCs in a lymphatic system in a rat model through PA imaging. We systematically examined and optimized a number of experimental parameters including the concentration, size, as well as surface charge of the AuNCs. We reduced the concentration of injected AuNCs down to 50 pM (40 times lower than our previous report, greatly reducing the potential toxicity of AuNCs) for SLN imaging, keeping a sufficient SNR. It was found that the 30-nm AuNCs exhibited a faster transport rate and a larger amount of accumulation in the SLN than the 50-nm AuNCs, but the latter generated stronger PA signals due to a larger optical absorption cross section. This result indicates that the 50-nm AuNCs a better contrast agent. As for AuNCs with different surface charges, their transport rates to SLNs decreased in the order of neutral > negative > positive. These results can serve as guidelines for choosing optimal parameters of AuNCs in metastatic lymph nodes mapping by noninvasive PA imaging.

## 5. ACKNOWLEDGMENTS

This work was sponsored by National Institutes of Health grants No. R01 EB000712, No. R01 EB008085, No. R01 CA134539, and No. U54 CA136398 (Network for Translational Research) (to L.V.W.). L.V.W. has a financial interest in Microphotoacoustics, Inc. and Endra, Inc., which, however, did not support this work.



Downloaded From: https://www.spiedigitallibrary.org/conference-proceedings-of-spie on 9/18/2018
Terms of Use: https://www.spiedigitallibrary.org/terms-of-use

## REFERENCES


[1] N. P. Alazraki, D. Eshima, L. A. Eshima, S. C. Herda, D. R. Murray, J. P. Vansant, A. T. Taylor, "The Sentinel Node Concept, and the Intraoperative Gamma Probe in Melanoma, Breast Cancer, and Other Potential Cancers," *Semin. Nucl. Med.* 27, 55–67 (1997).

[2] H. Kobayashi, S. Kawamoto, Y. Sakai, P. L. Choyke, R. A. Star, M. W. Brechbiel, N. Sato, Y. Tagaya, J. C. Morris, T. A. Waldmann, "Lymphatic Drainage Imaging of Breast Cancer in Mice by Micro-magnetic Resonance Lymphangiography Using a Nano-size Paramagnetic Contrast Agent," *J. Natl. Cancer Inst.* 96, 703–708 (2004).

[3] F. Amersi, N. M. Hansen, "The Benefits and Limitations of Sentinel Lymph Node Biopsy," *Curr. Treat. Options Oncol.* 7, 141–151 (2006).

[4] S. Krishnamurthy, N. Sneige, D. G. Bedi, B. S. Edieken, B. D. Fornage, H. M. Kuerer, S. E. Singletary, K. K. Hunt, "Role of Ultrasound-guided Fine-needle Aspiration of Indeterminate and Suspicious Axillary Lymph Nodes in the Initial Staging of Breast Carcinoma," *Cancer* 95, 982–988 (2002).

[5] L. V. Wang, "Multiscale Photoacoustic Microscopy and Computed Tomography," *Nat. Photonics* 3, 503–509 (2009).

[6] C. Kim, C. Favazza, L. V. Wang, "*In Vivo* Photoacoustic Tomography of Chemicals: High-Resolution Functional and Molecular Optical Imaging at New Depths," *Chem. Rev.* 110, 2756–2782 (2010).

[7] G. Ku, L. V. Wang, "Deeply Penetrating Photoacoustic Tomography in Biological Tissues Enhanced with an Optical Contrast Agent," *Opt. Lett.* 30, 507–509 (2005).

[8] A. G. Cuenca, H. Jiang, S. N. Hochwald, M. Delano, W. G. Cance, S. R. Grobmyer, "Emerging Implications of Nanotechnology on Cancer Diagnostics and Therapeutics," *Cancer* 107, 459–466 (2006).

[9] J. Chen, F. Saeki, B. J. Wiley, H. Cang, M. J. Cobb, Z. Y. Li, L. Au, H. Zhang, M. B. Kimmey, X. Li, Y. Xia, "Gold Nanocages: Bioconjugation and Their Potential Use as Optical Imaging Contrast Agents," *Nano Lett.* 5, 473–477 (2005).

[10] C. Kim, E. C. Cho, J. Chen, K. H. Song, L. Au, C. Favazza, Q. Zhang, C. M. Cobley, F. Gao, Y. Xia, L. V. Wang, "*In Vivo* Molecular Photoacoustic Tomography of Melanomas Targeted by Bioconjugated Gold Nanocages," *ACS Nano* 4, 4559–4564 (2010).

[11] Y. Sun, Y. Xia, "Mechanistic Study on the Replacement Reaction between Silver Nanostructures and Chloroauric Acid in Aqueous Medium," *J. Am. Chem. Soc.* 126, 3892–3901 (2004).

[12] K. H. Song, C. Kim, C. M. Cobley, Y. Xia, L. V. Wang, "Near-Infrared Gold Nanocages as a New Class of Tracers for Photoacoustic Sentinel Lymph Node Mapping on a Rat Model," *Nano Lett.* 9, 183–188 (2009).

[13]Q. Zhang, W. Li, L. P. Wen, J. Chen, Y. Xia, "Facile Synthesis of Ag Nanocubes of 30 to 70 nm in Edge Length with $CF_3COOAg$ as a Precursor," *Chem. Eur. J. 16*, 10234–10239 (2010).

[14] K. H. Song, L. V. Wang, "Deep Reflection-mode Photoacoustic Imaging of Biological Tissue," *J. Biomed. Opt.* 12, 060503 (2007).

[15] E. G. Soltesz, S. Kim, R. G. Laurence, A. M. DeGrand, C. P. Parungo, D. M. Dor, L. H. Cohn, M. G. Bawendi, J. V. Frangioni, T. Mihaljevic, "Intraoperative Sentinel Lymph Node Mapping of the Lung Using Near-Infrared Fluorescent Quantum Dots," *Ann. Thorac. Surg.* 79, 269–277 (2005).

[16] S. M. Moghimi, A. R. Rajabi-siahboomi, "Advanced Colloid-Based Systems for Efficient Delivery of Drugs and Diagnostic Agents to the Lymphatic Tissues," *Prog. Biophys. molec. Biol.* 65, 221–249 (1996).

[17] E. C. Cho, C. Kim, F. Zhou, C. M. Cobley, K. H. Song, J. Chen, Z. Li, L. V. Wang, Y. Xia, "Measuring the Optical Absorption Cross Sections of Au–Ag Nanocages and Au Nanorods by Photoacoustic Imaging," *J. Phys. Chem. C* 113, 9023–9028 (2009).

[18] S. M. Moghimi, A. R. Rajabi-siahboomi, "Advanced Colloid-Based Systems for Efficient Delivery of Drugs and Diagnostic Agents to the Lymphatic Tissues," *Prog. Biophys. molec. Biol.* 65, 221–249 (1996).




Downloaded From: https://www.spiedigitallibrary.org/conference-proceedings-of-spie on 9/18/2018
Terms of Use: https://www.spiedigitallibrary.org/terms-of-use